Multi-variable Optimization Methodology for Medium-frequency High-power Transformer Design Employing Steepest Descent Method

Annoy Kumar Das*, Zhongbao Wei†, Baylon G. Fernandes*, Haonan Tian†, Madasamy P. Thevar†,
Shuyu Cao†, Vaisambhayana B. Sriram†, Anshuman Tripathi† and Philip C. Kjær‡
†Energy Research Institute @NTU, Nanyang - 637141, Singapore,
Email: weizb,tianhn,madasamy,sycao,vsriram,antri@ntu.edu.sg
‡Vestas Wind System A/S, DK-8200, Arhus N, Hedeager, Denmark,
Email: pck@vestas.com
*Department of Electrical Engineering, Indian Institute of Technology - Bombay, Powai, Mumbai - 400076, India
Email: dasak,bgf@ee.iitb.ac.in

***Abstract*—To find balance among multiple design objectives of a medium/high-frequency (MF/HF) high-power (HP) transformer is best addressed employing an optimization technique. In this paper, MF HP transformer design is formulated as a multi-variable optimization problem, where efficiency, power density and temperature rise are chosen as design objectives. Total loss, core volume and maximum temperature rise are modeled as respective cost functions and amalgamated using weighted-sum approach to derive objective function. It is minimized using Steepest descent method. Being a gradient-based search technique, it preserves correlation among design variables during minimization. Using the proposed methodology, optimal design of a 10 kW, 0.5/5 kV, 1 kHz natural oil-cooled transformer with amorphous core and concentric foil winding, is derived. It is estimated to have an efficiency of 99.55% at a power density of 19.79 and maximum node temperature of 52.92 °C. These merit of figures are validated using FEM and CFD studies. Cost-effectiveness of proposed methodology is discussed with the help of a hardware prototype, built from off-the-shelf amorphous core. Benefits like design flexibilities and plausible cost-effectiveness, are inherent to gradient-based optimization method, which augur well for its applicability for MF HP transformer design.**

***Index Terms*—Cost function, gradient-based optimization, high-power, medium-frequency, Steepest descent, weighted-sum**

I. Introduction

Design of a medium/high-frequency (MF/HF) high-power (HP) transformer has drawn much attention in recent times, culminating in higher power density, compact size, etc. [1]. Applications, having space and/or weight constraint, are most benefited e.g. railway traction [2], offshore wind farm [3], solid state transformer (SST) [4] etc. Higher frequency relates to lesser volume of magnetics but enhanced core and winding losses, which necessitates to have better thermal management. Simultaneous improvement in both efficiency (η) and power density (pd) are in contrast with each other. With higher flux density (B_c) in the core, winding size and hence losses decrease but core loss increases. While B_c is lowered, core volume (V_{core}) increases and power density decreases. To find a balance among multiple design objectives and attain optimal performance of MF HP transformer is best addressed employing an optimization methodology.

An elaborate survey of transformer designs, encompassing a wide range of frequencies and its optimization, is found in [5]. Single-variable optimization method is adapted in [6], [7], where objective function is translated and minimized with respect to a single design variable using method of elimination. But it requires extensive mathematical modeling. Library-based optimization algorithm of MF HP transformer design is encountered in [8]–[13]. Based on combinations of core and winding materials, all feasible designs are evaluated and thereby an optimal design is chosen. In [13], the concept of weighted-sum approach is explored to select optimal design based on multiple design objectives e.g. weight, loss and leakage inductance. Implementation of library-based technique is associated with a heavy computational burden because of exhaustive combinations of free parameters [10], [11]. Also material libraries of core and winding should be appropriate for the desired power rating or else derived transformer design may not be optimal in nature.

In this paper, a multi-variable gradient-based optimization method is explored to derive optimal design of MF HP transformer. Efficiency, power density and temperature rise are chosen as design objectives. Total loss, core volume and maximum temperature rise are modeled as respective cost functions, which are shown to be explicit functions of design variables, thereby guaranteeing applicability of gradient-based approach. Using weighted-sum approach, objective function is derived and minimized employing Steepest descent method. A 10 kW, 0.5/5 kV, 1 kHz natural oil-cooled transformer is optimally designed and validated with FEM and CFD studies. A hardware prototype of similar rating is built using off-the-shelf amorphous core and compared to show cost-effectiveness of proposed method. Performance indices of optimal design lie in close vicinity of similar figures reported in literature, which substantiates that proposed optimization methodology performs satisfactorily for MF HP transformer design.

978-1-5386-1180-7/18/$31.00 ©2018 IEEE

TABLE I
DESIGN SYSTEM PARAMETERS

Parameters	Value
Nominal power (P_o)	10 kW
Switching frequency (f_s)	1 kHz
Excitation voltages (V_1/V_2)	0.5/5.0 kV
Rated currents (I_1/I_2)	20.86/2 A

II. OPTIMIZATION METHODOLOGY

A. System parameters

System parameters $[U_{sys}]$, for said transformer design, are summarized in (1). Nominal power (P_o) is 10 kW. Primary and secondary rms voltages (V_1, V_2) and currents (I_1, I_2) are given in Table I. Switching frequency (f_s) of 1 kHz is chosen. Coolant is mineral oil with an ambient temperature of 20 °C.

$$\begin{bmatrix} U_{sys} \\ U_{fix} \\ \\ x \end{bmatrix} = \left[\begin{array}{cccccc} V_1 & I_1 & V_2 & I_2 & f_s & P_o \\ w_1 & h_1 & t_1 & d_1 & d_{sp} & d_{bn} \\ w_2 & h_2 & t_2 & d_2 & & \\ \hline \mathbf{E} & \mathbf{T} & \mathbf{B_c} & \mathbf{n_1} & & \end{array}\right] \tag{1}$$

B. Fixed parameters

Prior to commencement of iterative algorithm depicted in Fig. 4, core and conductor material and its geometry are fixed at user's discretion, summarized by $[U_{fix}]$ in (1). Fig. 1(a) shows an EE core, derived from two amorphous U cores [14]. Bobbin thickness is given by d_{bn}. Shell type concentric winding is shown in Fig. 1(b), where primary (red) is placed inside with secondary (blue) outside. Copper foil conductor is used for both windings. Primary foil has width (w_1), height (h_1) and insulation thickness (t_1) of 0.25, 25 and 0.001 mm respectively. Secondary foil has width (w_2), height (h_2) and insulation thickness (t_2) of 0.25, 5 and 0.001 mm respectively. Nomex (410) is used as intra- and inter-winding insulation to support desired electrostatic potential [15]. Its thickness d_1 and d_2 in primary and secondary windings are 0.05 and 0.18 mm respectively. Spacer of thickness d_{sp} is considered for better heat exchange among winding sections and coolant.

C. Design variables

Out of many free parameters, core central limb thickness and depth (E, T), flux density (B_c) and primary layers (n_1) are identified as independent design variables $[x]$, summarized in (1). Using comprehensive mathematical framework, remaining free parameters and subsequently cost functions are shown to be explicitly deducible with respect to $[x]$. Thereby, it ensures applicability of gradient-based optimization method to minimize derived objective function (f_{obj}).

D. Deduction of free parameters

1) Core geometry: EE core assembly with front and side views are shown in Fig. 1(a). Remaining core dimensions are deduced with respect to design variables $[x]$ and shown in Fig. 1(b). For amorphous core, effective core area (A_e) is less

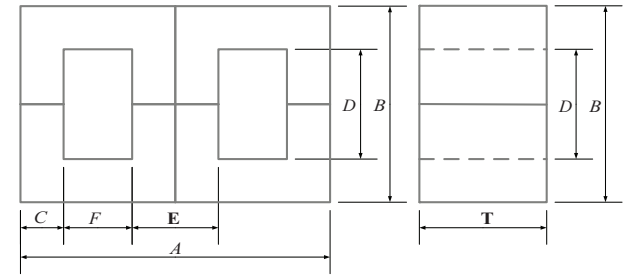

(a)

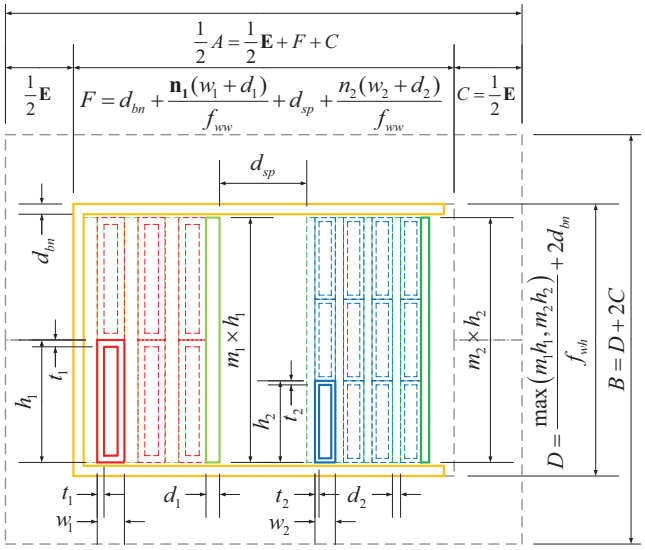

(b)

Fig. 1. Geometry deduction with respect to design variables (a) core: front and side views (b) winding: primary (red) and secondary (blue)

than its geometric area (A_c) and calculated using (2a), where lamination factor (l_f) of ≈ 0.84 is assumed [14].

$$\left[\begin{array}{c|c} A_c & A_e \end{array}\right] = \left[\begin{array}{c|c} \mathbf{ET} & l_f A_c \end{array}\right] \tag{2a}$$

$$\left[\begin{array}{c|c|c} N_1 & m_1 & n_1 \end{array}\right] = \left[\begin{array}{c|c|c} \frac{V_1}{4k_f f_s \mathbf{B_c} A_c} & \frac{N_1}{\mathbf{n_1}} & \mathbf{n_1} \end{array}\right] \tag{2b}$$

$$\left[\begin{array}{c|c|c} N_2 & m_2 & n_2 \end{array}\right] = \left[\begin{array}{c|c|c} N_1 \frac{V_2}{V_1} & \frac{D-2d_{bn}}{f_{wh} h_2} & \frac{N_2}{m_2} \end{array}\right] \tag{2c}$$

2) Winding geometry: Fig. 1(b) depicts winding disposition and its relevant deduction of geometry. Primary turns (N_1) and turns per layer (m_1) are known from (2b). For sinusoidal excitation, form factor (k_f) is 1.11. Secondary turns (N_2), turns per layer (m_2) and number of layers (n_2) are calculated sequentially using (2c). While core window height and width (D, F) are deduced, filling factors f_{wh}, f_{ww} are used for winding height and width respectively to take manufacturing tolerance into account. This iterative process reflects inherent correlation among core and winding design parameters, which is employed to the designers' advantage during multi-variable gradient-based optimization. Deduction of design parameters, governed by equations in (2) ensures that area product (A_p) criterion of derived core geometry is always satisfied.

E. Loss calculation

1) Core loss: Original Steinmetz Equation (OSE) [16] is best suited to calculate core loss, when excitation is sinusoidal in nature and only fundamental frequency is present. It is computationally cheap and employs only material properties. In this design, amorphous alloy 2605SA1 is chosen, which exhibits saturation flux density (B_{sat}) of 1.56 T and loss coefficients K, α and β of 1.377, 1.51 and 1.74 respectively [14]. Employing OSE method, core loss per unit volume (p_v) is obtained, given by (3a). With shell type winding, heat exchange processes involved in core central and external limbs are different. It necessitates core to be differentiated into separate thermal branches, which would yield more accurate estimation of node temperature. Thus core volumes (V_{cc}, V_{ce}) as well as losses (P_{cc}, P_{ce}) are calculated separately for central and external limbs using (3b) and (3c) respectively.

$$p_v = K f_s^{\alpha} \mathbf{B_c}^{\beta} \tag{3a}$$

$$\left[\begin{array}{c:c} V_{cc} & V_{ce} \end{array}\right] = \left[\begin{array}{c:c} \mathbf{E}D & \mathbf{E}(A+D-\mathbf{E}) \end{array}\right] \mathbf{T} \tag{3b}$$

$$\left[\begin{array}{c:c} P_{cc} & P_{ce} \end{array}\right] = p_v \left[\begin{array}{c:c} V_{cc} & V_{ce} \end{array}\right] \tag{3c}$$

2) Winding loss: Accurate calculation of winding resistance is essential to loss and efficiency estimation. DC resistance (R_{dc_i}) at i^{th} layer is found using (4a). Dynamic change in wire resistivity (ρ_x) with increase in winding temperature (T_x) is implied by (4b), where ρ_{20} and α_{Cu} are resistivity at 20 °C and temperature coefficient of resistance respectively. This correction is implemented in an iterative manner so that winding temperatures and hence losses, calculated at convergence, are accurate in nature. Foil area (a) is calculated using (4c). Preceding section's half-perimeter (d_0) is given by (4d) for primary and secondary windings. It is used to calculate mean length of turn (MLT_i) of i^{th} layer, shown in (4e).

$$R_{dc_i} = \frac{\rho_x m}{a} MLT_i \tag{4a}$$

$$\rho_x = \rho_{20}\left[1 + \alpha_{Cu}(T_x - T_{20})\right] \tag{4b}$$

$$a = (w - 2t)(h - 2t) \tag{4c}$$

$$\left[\begin{array}{c} d_{op} \\ \hdashline d_{os} \end{array}\right] = \left[\begin{array}{c} \mathbf{E} + \mathbf{T} \\ \hdashline d_{op} + 4\left[\mathbf{n_1}(w_1 + d_1) + d_{sp}\right] \end{array}\right] \tag{4d}$$

$$\begin{aligned} MLT_i &= 2\left[d_0 + 4(i-1)(w+d)\right] + 4w \\ &= \left[\begin{array}{c:c} a_1 i & a_0 \end{array}\right] \end{aligned} \tag{4e}$$

$$\left[\begin{array}{c:c} a_1 & a_0 \end{array}\right] = \left[\begin{array}{c:c} 8\,(w+d) & (2d_o - 4w - 8d) \end{array}\right] \tag{4f}$$

Foil winding ac resistance (R_{ac}) and its' factor (F_R) are calculated using Dowell's expression [17]. Relative error in F_R estimation is kept to minimum if conductor thickness (w) to skin depth (δ) ratio is kept low and winding porosity factor (η_w) is high [18]. At f_s= 1 kHz, δ is 2.09 mm at an ambient of 20 °C. Thus foil thickness of 0.25 mm is chosen to keep ac effect minimal. Very high η_w is difficult to meet in practice due to stringent dielectric requirement in high-voltage (HV) design and to allow for manufacturing tolerance. In [19], effect of winding porosity is accommodated through modification of penetration factor (Δ). Likewise, a correction factor of $\sqrt{\eta_w}$ is introduced along with basic Dowell's expression in (5b). With these correction factors and proper selection of core and winding geometries, Dowell's method yields fairly accurate estimation of foil ac resistance at medium switching frequency, which is also discussed at length in [20].

$$\delta = \frac{1}{\sqrt{\pi f \mu \sigma}} \tag{5a}$$

$$\Delta = \frac{w - 2t}{\delta}\sqrt{\eta} \tag{5b}$$

$$\zeta_1 = \frac{\sinh(2\Delta) + \sin(2\Delta)}{\cosh(2\Delta) - \cos(2\Delta)} \tag{5c}$$

$$\zeta_2 = \frac{\sinh(\Delta) - \sin(\Delta)}{\cosh(\Delta) + \cos(\Delta)} \tag{5d}$$

$$\begin{aligned} F_{R_i} &= \Delta\left[\zeta_1 + \frac{2}{3}\left(i^2 - 1\right)\zeta_2\right] \\ &= \Delta\left[b_2 i^2 + b_1 i + b_0\right] \end{aligned} \tag{5e}$$

$$\left[\begin{array}{c:c:c} b_2 & b_1 & b_0 \end{array}\right] = \left[\begin{array}{c:c:c} \frac{2}{3}\zeta_2 & 0 & \zeta_1 - \frac{2}{3}\zeta_2 \end{array}\right] \tag{5f}$$

Skin depth (δ) is found using expression in (5a), where σ and μ are wire conductivity and permeability respectively. Factors due to skin and proximity effects are identified using (5c) and (5d) respectively. (5e) helps calculate ac resistance factor (F_{R_i}) at i^{th} foil layer. For algebraic brevity, MLT_i and F_{R_i} are expressed as polynomials of layer number (i) in (4e) and (5e). This helps deduce ac resistance (R_{ac_i}) at i^{th} layer as a function of layer number (i), which upon simplification reduces to a 3^{rd} order polynomial. Total winding ac resistance (R_{ac}) is obtained using (6a), where individual layer R_{ac_i} are summed together. Coefficient matrices $[a]$, $[b]$ and $[c]$ are summarized in (4f), (5f) and (6b) respectively.

$$\begin{aligned} R_{ac} &= \sum_{i=1}^{n} R_{ac_i} = \sum_{i=1}^{n} R_{dc_i} \times F_{R_i} \\ &= \frac{\rho_x m \Delta}{a} \sum_{i=1}^{n} \left(c_3 i^3 + c_2 i^2 + c_1 i + c_0\right) \\ &= \frac{\rho_x m \Delta}{a} \begin{bmatrix} c_3 \\ c_2 \\ c_1 \\ c_0 \end{bmatrix}^{\mathbb{T}} \begin{bmatrix} \left(\frac{n(n+1)}{2}\right)^2 \\ \frac{n(n+1)(2n+1)}{6} \\ \frac{n(n+1)}{2} \\ n \end{bmatrix} \end{aligned} \tag{6a}$$

$$\left[\begin{array}{c:c} c_3 & c_2 \\ \hdashline c_1 & c_0 \end{array}\right] = \left[\begin{array}{c:c} b_2 a_1 & \begin{pmatrix} b_2 a_0 \\ +b_1 a_1 \end{pmatrix} \\ \hdashline \begin{pmatrix} b_1 a_0 \\ +b_0 a_1 \end{pmatrix} & b_0 a_0 \end{array}\right] \tag{6b}$$

$$\left[\begin{array}{c:c} P_p & P_s \end{array}\right] = \left[\begin{array}{c:c} I_1^2 R_{ac_1} & I_2^2 R_{ac_2} \end{array}\right] \tag{6c}$$

Calculation of MLT_i relies on core width and depth (E, T) along with primary layers (n_1). Thus (6c) clearly shows that R_{ac} and hence winding losses (P_p and P_s) are deducible as explicit functions with respect to design variables $[x]$.

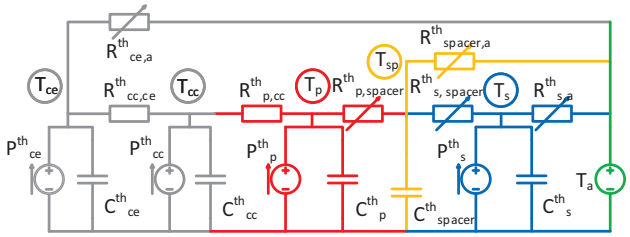

Fig. 2. Equivalent thermal network of a MF HP transformer assembly of EE core (gray) and concentric winding sections i.e. primary (red), secondary (blue) and inter-winding spacer (orange), all connected to ambient (green)

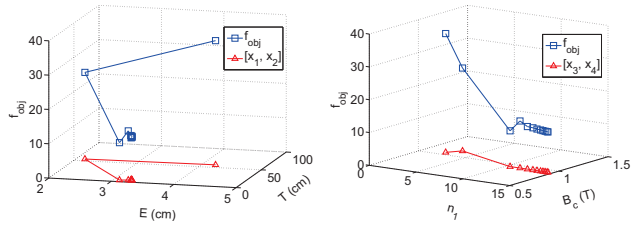

Fig. 3. In Steepest descent method, with increasing number of iterations objective function is minimized and simultaneous corrections are applied on design variables (a) core width and depth (b) flux density and primary layers

F. Node temperature estimation

Once the losses are known, its impact on thermal model of core and winding is investigated. A MF HP transformer encompasses a wide variety of materials e.g. core, conductor, insulation, coolant, which altogether exhibit a heterogeneous thermal behavior, dictated by surface area, material properties and exposure to coolant [9]–[11], [21]. Individual thermal branches are derived for EE core and concentrated windings and concatenated to obtain an equivalent thermal network of MF HP transformer, shown in Fig. 2. Detailed study of said thermal model and its verification are presented in [22].

Core (gray) is differentiated into central (Cc) and external (Ce) limbs as heat exchange mechanisms are diverse, leading to varied degree of temperature rises. Heat transfer is mainly conductive in core central (Cc) limb and convective in core external (Ce) limbs. In a (P, S) winding disposition, primary (red) is placed nearer to core while secondary (blue) is placed outside, leading to better exposure to coolant surface. In-between winding sections, spacer (orange) facilitates better heat exchange among winding sections and coolant. It is modeled as an additional thermal node in the equivalent network, shown in Fig. 2, to obtain higher accuracy.

$$[G^{th}] = \left[\begin{array}{cc:ccc} G^{th}_{core} & & G^{th}_{p,cc} & 0 & 0 \\ & & 0 & 0 & 0 \\ \hdashline G^{th}_{p,cc} & 0 & & & \\ 0 & 0 & & G^{th}_{wdg} & \\ 0 & 0 & & & \end{array}\right] \tag{7a}$$

$$[P^{th}] = \left[\begin{array}{cc:ccc} P_{cc} & P_{ce} & P_p & 0 & P_s \end{array}\right]^{\mathbb{T}} \tag{7b}$$

$$[\Delta T] = -[G^{th}]^{-1}[P^{th}] \tag{7c}$$

System matrices e.g. thermal conductance $[G^{th}]$ and losses $[P^{th}]$ are calculated employing (7a) and (7b) respectively. Individual thermal conductance (G^{th}_{ij}) is calculated as $1/R^{th}_{ij}$. Steady-state energy balance equations at respective thermal nodes for core and windings are expressed concisely in (7c). It is numerically solved using numerical approach e.g. Modified Euler (Heun's) method to find node temperature rises $[\Delta T]$. System matrices are updated in each iteration according to change in $[\Delta T]$ to mimic heat transfer process accurately. Detail discussion of dynamic correlation between winding temperature rise and increase in copper losses due to change in wire resistivity is presented in [22].

G. Formulation of cost and objective functions

Efficiency (η), power density (pd) and temperature rise (ΔT) are chosen as design objectives. Concurrently total loss (P_{loss}), core volume (V_{core}) and maximum temperature rise (ΔT_{max}) are configured as cost functions, given by (8a). Employing weighted-sum approach, cumulative objective function (f_{obj}) is derived from multiple cost functions, shown in (8b). As individual cost functions are previously shown to be explicit functions of design variables $[x]$, the same follows for f_{obj}. It also guarantees applicability of gradient-based search technique to minimize f_{obj} and find an optimal solution. Allocation of individual weight defines affinity of desired solution onto respective design objectives. To encompass a broader solution space, each weight is varied uniformly within a bound of (0,1) and subjected to equality constraint in (8c).

$$\left[\begin{array}{c} f_1 \\ \hdashline f_2 \\ \hdashline f_3 \end{array}\right] = \left[\begin{array}{c} P_{loss} \\ \hdashline V_{core} \\ \hdashline \Delta T_{max} \end{array}\right] = \left[\begin{array}{c} (P_{cc} + P_{ce}) + (P_p + P_s) \\ \hdashline (V_{cc} + V_{ce}) \\ \hdashline (\Delta T_{core} + \Delta T_{winding}) \end{array}\right] \tag{8a}$$

$$[f_{obj}] = w_{loss} f_1 + w_{vol} f_2 + w_{\Delta T} f_3 \tag{8b}$$

$$1 = \sum (w_{loss} + w_{vol} + w_{\Delta T}) \tag{8c}$$

H. Minimization using Steepest descent method

It utilizes gradient information to determine search direction to minimize objective function (f_{obj}) [23]. Gradient vector $[\nabla f(x)]$ is computed using central difference method. In each iteration, correction vector $[\alpha \nabla f(x_i)]$ is used to update design variables. Convergence criteria is met when absolute increment in objective function $\left(|fx_{i+1} - fx_i|\right)$ or its norm $\left(\|\nabla f(x_i)\|\right)$ is less than tolerance limits ϵ_1 and ϵ_2 respectively. Fig. 3 depicts that value of f_{obj} decreases gradually in successive iterations until convergence criteria is fulfilled. Simultaneous corrections in design variables i.e. core central limb width and depth (E, T) and flux density and primary layers (B_c, n_1) are shown in Fig. 3(a) and Fig. 3(b) respectively. Gradient-based search technique is able to make concurrent corrections on multiple design variables $[x]$, that helps attain a balanced design where core and copper losses are nearly equal, thus optimum efficiency is reached at rated output.

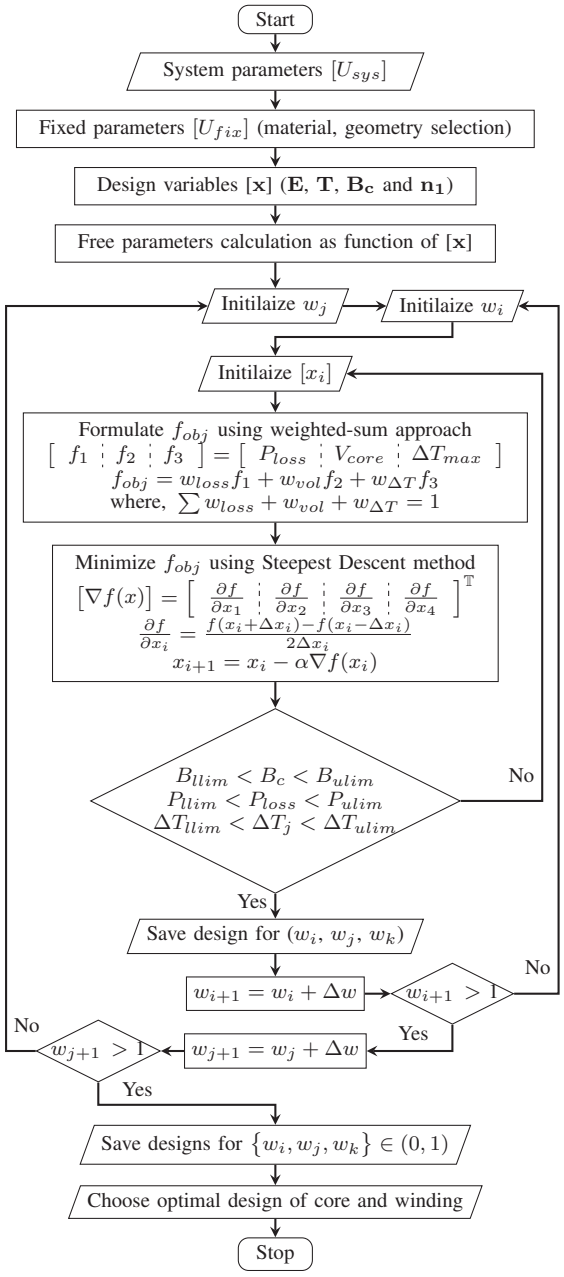

Fig. 4. Framework of optimization methodology (suffix i, j, k imply weight indices for total loss, core volume and maximum temperature rise respectively)

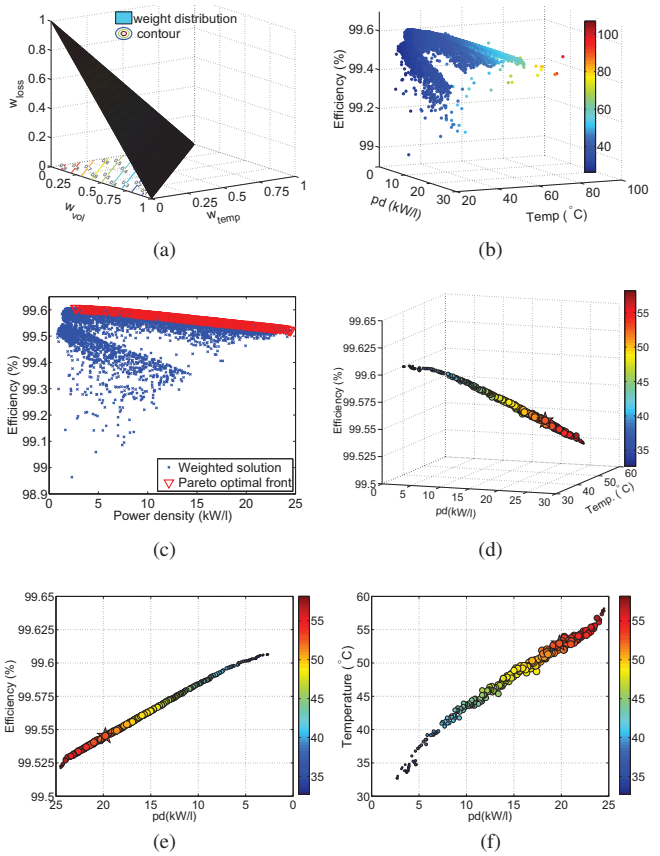

Fig. 5. Optimal design selection and trade-off among objectives (a) weight distribution (b) pool of weighted designs (c) non-dominated designs (d) pareto optimal front and preferred design (e) trade-off between efficiency and power denisty (f) trade-off between node temperature and power density

III. Optimal Design Selection

A. Pareto optimal front

Framework of multi-variable optimization methodology is outlined in Fig. 4. Individual weights e.g. w_{loss}, w_{pd} and $w_{\Delta T}$ are assigned for total loss (P_{loss}), core volume (V_{core}) and maximum temperature rise (ΔT) respectively. Using inner and outer algebraic loops, each of weights w_{loss} and w_{pd} is varied within span of (0,1). Subjected to constraint (8c), weight distribution is derived and shown in Fig. 5(a), which depicts varying degrees of affinities to each cost function. For each combination in weight distribution, objective function (f_{obj}) is formulated and minimized, culminating in a pool of weighted designs. Fig 5(b) shows scatter plot of the same with respect to efficiency (η), power density (pd) and maximum node temperature (T_{max}), where each marker signifies one weighted design. While derived designs are plotted in Fig. 5(c) with respect to η and pd, it is seen that certain solutions are superior to the rest, in at least one design objective. Fig. 5(d) shows these non-dominated solutions, isolated with respect to efficiency and power density and constitutes pareto optimal front for said MF HP transformer design.

B. Trade-off among design objectives

In this design example, maximum efficiency (η_{max}) of 99.61% is attained at minimum power density (pd_{min}) of 2.65 kW/l and maximum node temperature of 32.68 °C. From observed data, it is inferred that increased core surface helps attain better thermal management but adversely affects power density. Fig. 5(e) shows that efficiency decreases as power density increases, which is attributed to enhanced loss density as core and winding volume are reduced. Maximum power density (pd_{max}) of 24.49 kW/l is achieved at an efficiency of 99.52% and maximum node temperature of 58.16 °C.

TABLE II
PERFORMANCE INDICES OF OPTIMAL DESIGN (A) GRADIENT-BASED (B) LIBRARY-BASED (C) EXPERIMENTAL PROTOTYPE

Parameters	Optimal design
Nominal power (P_o)	10 kW
Rated frequency (f_s)	1 kHz
Excitation voltages (V_{LV}/V_{HV})	0.5/5.0 kV
Core selection	Amorphous (2605SA1)
Conductor	Foil
Coolant	Natural-oil
Efficiency (η)	99.55%
Power density (pd)	19.79 kW/l
Temperature rise (ΔT)	32.92 °C

(a)

Shuai *et al.* [9]	Bahmani *et al.* [10]	Bahmani *et al.* [11]
25 kW	50 kW	50 kW
4 kHZ	5 kHz	5 kHz
0.4/2.4 kV	1/3 kV	1/3 kV
Nanocrystalline (VITREPERM500F)	Nanocrystalline (VITREPERM500F)	Ferrite (3C85)
Litz	Litz	Litz
Forced-air	Natural-air	Natural-air
99.54%	99.66%	99.48%
8.00 kW/l	15.1 kW/l	11.5 kW/l
68.5 °C [a]	60 °C	60 °C

(b)

Experimental prototype
10 kW
1 kHz
0.5/5.0 kV
Amorphous (2605SA1)
Round
Natural-oil
99.11%
14.33 kW/l
–

(c)

[a] Ambient temperature of 30 °C is assumed

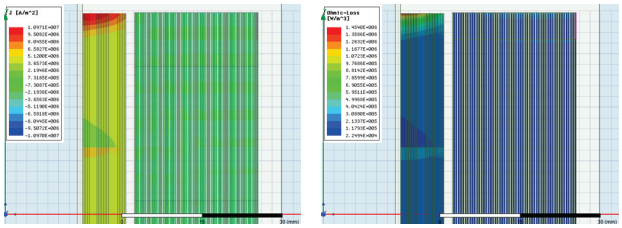

(a) (b)

Fig. 6. Winding loss modeling in FEM (a) Current density (b) Loss density

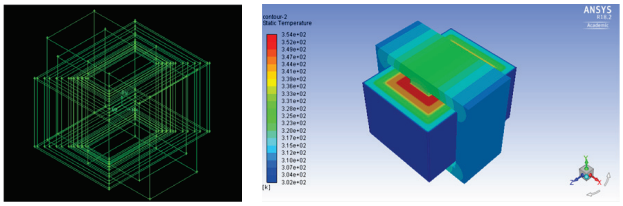

(a) (b)

Fig. 7. Thermal modeling in CFD (a) mesh construction of core and winding assembly (b) isometric view of volumetric temperature distribution in Kelvin

Fig. 5(f) depicts that node temperature tends to increase with higher power density. These observations lie in agreement with general trends seen in MF/HF transformer design and corroborates the legitimacy and aptness of proposed gradient-based multi-variable optimization methodology.

C. Optimal design selection and Discussion

Based on trade-off among design objectives e.g. efficiency (η), power density (pd) and maximum temperature rise (ΔT), an optimal solution is chosen, which is shown as starred among pareto front solutions in Fig. 5(d). Derived EE core has following dimensions in mm e.g. A=130.7, B=112.5, C=13.6, D=85.3, E=27.2 and T=61.6. Optimal flux density (B_c) is obtained as 0.9872 T. Primary foil winding has 81 turns (N_1), arranged in 3 coils (m_1), each having 27 layers (n_1). Secondary foil winding has 810 turns (N_2), divided into 15 coils (m_2), each having 54 layers (n_2). At nominal output power of 10 kW, estimated core and copper losses are 23.1 W and 22.6 W respectively. It demonstrates that proposed method is able to find optimal solution such that individual core and copper losses are almost equal and ideally maximum efficiency is achieved when transformer delivers rated power.

For selected material and geometry of core, conductor and insulation, optimal design is estimated to have an efficiency (η) of 99.55% at a power density (pd) of 19.79 and maximum node temperature of 52.92 °C, which are shown in Table II(a). Thus maximum temperature rise (ΔT) is limited to 32.92 °C, as coolant temperature is assumed 20 °C. Similar performance indices, found in literature of MF/HF transformer designs, are also shown in Table II(b) [9]–[11]. Although it is difficult to adjudge these merit of figures because said designs are derived with diverse system requirements, a cursory comparison would help understand aptness of derived optimal design parameters. At same kVA rating, foil winding width tends to be higher, compared to litz or round wires, which necessitates to design core with larger window area and adversely affects power density. Transformer mineral oil, being a better coolant than air due to its superlative convective properties, helps achieve better thermal management. Consequently it also enhances power density as higher loss density is accommodated for same degree of temperature rise in core and windings. Table II depicts that performance indices of derived optimal design lies in the vicinity of library-based designs' parameters, thereby indicates that proposed gradient-based optimization method performs satisfactorily for MF HP transformer design.

IV. OPTIMAL DESIGN VALIDATION WITH FEM, CFD

To validate performance indices of derived optimal design, 2D axisymmetric FEM simulation is carried out in Maxwell [24] to accurately calculate core and copper losses. Current and loss density distribution across individual layer of foil windings are shown in Fig. 6(a) and Fig. 6(b) respectively.

TABLE III
VALIDATION OF ANALYTICAL RESULTS WITH FEM, CFD (A) LOSS CALCULATION (B) THERMAL MODELING

Model	P_c	P_{Cu}
CFD	21.62	31.80
Analytical	23.06	22.63

(a)

T_{Cc}	T_{Ce}	T_p	T_s
64.75	42.64	79.90 81.90 82.29	69.35 58.46 43.21
50.04	37.32	52.92	47.83

(b)

As foil thickness is judiciously chosen, eddy-current effects in multi-layer windings are kept to be minimal, which also manifests in form of uniform loss density. Losses derived from FEM are used as input for CFD analysis in Fluent [24]. In current CFD model, 27 layers in primary are grouped into three lumped-layers e.g. (1-9), (10-18) and (19-27). Similarly 54 layers in secondary are grouped into three lumped-layers e.g. (1-18), (19-36) and (37-54). Intricate mesh configuration of said lumped layers is depicted in Fig. 7(a). Volumetric distribution of core and winding temperatures at steady-state is depicted in Fig. 7(b). Temperature rise in core central limb and primary winding is higher compared to core external limb and secondary winding, as they are less exposed to coolant and heat exchange is mainly conductive in nature.

Analytical and CFD simulations results are given in Table III. Core loss estimation matches very well with FEM result. But copper loss estimation indicates moderate deviation. It also adversely affects temperature rise estimation, particularly for primary, which being the low voltage (LV) winding, carries higher current and is major seat of heat source. FEM results show an efficiency of 99.47% with total loss of 53.42 W, compared to estimated efficiency of 99.55% with total loss of 45.69 W. The relative deviation is seen to be minimal ($\approx$ 0.08%) and substantiates feasibility of derived optimal design parameters in terms of efficiency and power density.

V. CASE STUDY WITH AN EXPERIMENTAL PROTOTYPE

Governed by design constraints in (1), a prototype is built using off-the-shelf amorphous core (AMCC0250), available from Hitachi [14]. It has following dimensions in mm e.g. A=126, B=128, C=19, D=90, E=38 and T=60. Solid round wires of standard gauze AWG 10 and 18 are used for primary and secondary windings respectively. Considering an operating flux density of 1.03 T, area-product method is implemented to derive winding parameters. Primary winding has 58 turns (N_1), arranged in 2 layers (n_1), each having 29 turns per layer (m_{p1}). Secondary winding has 594 turns (N_2), divided into 9 layers (n_2) with 66 turns (m_2) in each layer.

Transformer assembly and its oil-cooled thermal chamber are shown in Fig. 8 along with experimental setup. Built-prototype is subjected to extensive open-circuit (OC) and short-circuit (SC) tests, experimental results being shown in Fig. 9(a) and Fig. 9(b) respectively. During OC test, measured core loss is 39.1 W compared to estimated value of 30 W. During SC test, measured copper loss at rated operating

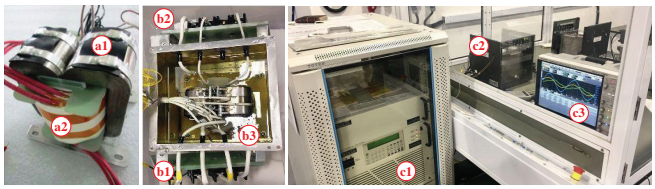

(a) (b) (c)

Fig. 8. Experimental prototype and test setup (a) transformer core (a1) and winding (a2) assembly during manufacturing stage (b) thermal chamber (b3) filled with midel oil while primary and secondary terminals (b1 and b2) are brought out for electrical connection (c) experimental setup comprising of power source (c1), transformer assembly (c2), digital oscilloscope (c3)

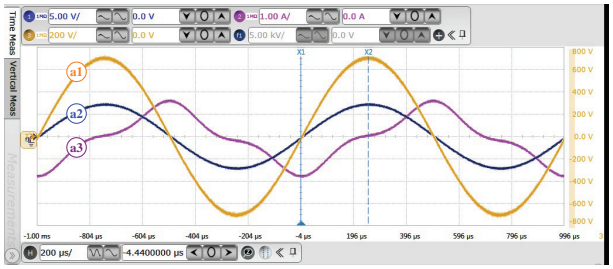

(a)

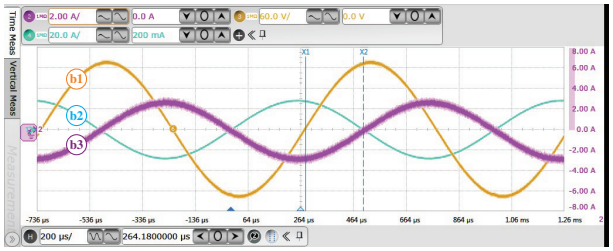

(b)

Fig. 9. Experimental results for loss measurement (a) open-circuit (OC) test showing primary and secondary (a1 and a2) voltages along with magnetizing (a3) current (b) short-circuit (SC) test showing applied voltage (b1) and currents in primary and secondary (b2 and b3) windings

condition is 50.24 W compared to estimated value of 43 W. Input power factor is found to be 0.187 ($\phi = 79.2\ °$), implying dominant inductive nature of winding impedance at high switching frequency. The experimental results show 99.11% efficiency with total loss of 89.34 W, compared to calculated efficiency of 99.27% with estimated total loss of 73 W. The relative deviation between measured and estimated efficiency is minimal ($\approx$ 0.16%) and suggests a high modeling accuracy of loss and temperature estimation methods implemented here.

Performance indices of optimal design and experimental prototype are presented in II(a) and II(c) respectively. Optimal design exhibits higher efficiency on account of balanced loss distribution i.e. core and copper losses are nearly equal. Experimental-prototype, built from off-the-shelf amorphous core, exhibits a volume and window area of 0.698 litre and 22.5 mm^2. Core with optimal geometry at same kVA rating exhibits a volume and window area of 0.505 litre and 32.54 mm^2, thereby offering a reduction of 38.2% in core

volume and increase of 30.86% in core window area. Thus optimal design also implies cost-effectiveness in terms of saving in core material due to less volume and weight. Derived geometry of optimal core also helps achieve better power density for the same kVA rating of designed transformer. These benefits, inherent to gradient-based optimization, augur well for its applicability for MF/HF transformer design.

VI. Conclusion

In this paper, multi-variable optimization method is explored to obtain optimal design of a medium-frequency (MF) high-power (HP) transformer. Steepest descent method, being a gradient-based search technique, conserves correlation among multiple design variables while minimizing derived objective function, thereby helps attain balance among multiple cost functions. It is generic in nature i.e. easily adapted and extended to different winding and core designs by partly modifying corresponding objective function.

Using proposed methodology, one can derive optimal design parameters of core and winding based on design specifications and material selection only. Core with optimal dimensions, if synthesized from amorphous or nanocrystalline alloy, would help adhere to optimum performance in terms of efficiency, power density as well as cost-effectiveness. Due to its discrete nature, manufacturers' off-the-shelf cores do not offer these flexibilities. Derived design parameters can also serve as an excellent starting guess for library-based search technique and confine solution space, saving time and effort.

Using proposed framework of optimization algorithm, an optimal design of 10 kW, 0.5/5.0 kV, 1 kHz natural oil-cooled transformer is derived. It is estimated to have an efficiency of 99.55% with a power density of 19.79 and maximum node temperature of 52.92 °C. These figure of merits are corroborated with the help of FEM and CFD studies, which exhibits an efficiency of 99.47%, indicating minimal deviation ($\approx$ 0.08%) in analytical estimation. Modeling accuracy is also validated using an experimental prototype, built with off-the-shelf core. With comparison to the later, optimally derived core offers a reduction of 38.2% in core volume and increase of 30.86% in core window area. Therefore it pronounces plausible cost-effectiveness due to less volume and weight of core material. Close agreement among analytical modeling, FEM, CFD studies and experimental validation, substantiates that gradient-based optimization methodology performs satisfactorily for medium/high-frequency (MF/HF) high-power (HP) transformer design.

Acknowledgment

Authors extend their gratitude to Vestas Wind System A/S, Denmark and Energy Research Institute@NTU, Nanyang, Singapore and Indian Institute of Technology, Bombay, India for accommodating above research work.

References

[1] E. Agheb and H. K. Hidalen, "Medium frequency high power transformers, state of art and challenges," in *2012 Int. Conf. on Renewable Energy Research and Applicat. (ICRERA)*, Nov 2012, pp. 1–6.

[2] D. Dujic, F. Kieferndorf, F. Canales, and U. Drofenik, "Power electronic traction transformer technology," in *Proc. of The 7th Int. Power Electron. and Motion Control Conf.*, vol. 1, June 2012, pp. 636–642.

[3] G. Ortiz, J. Biela, D. Bortis, and J. W. Kolar, "1 megawatt, 20 khz, isolated, bidirectional 12kv to 1.2kv dc-dc converter for renewable energy applications," in *The 2010 Int. Power Electron. Conf. - ECCE ASIA -*, June 2010, pp. 3212–3219.

[4] Y. Du, S. Baek, S. Bhattacharya, and A. Q. Huang, "High-voltage high-frequency transformer design for a 7.2kv to 120v/240v 20kva solid state transformer," in *IECON 2010 - 36th Annu. Conf. on IEEE Ind. Electron. Soc.*, Nov 2010, pp. 493–498.

[5] E. I. Amoiralis, M. A. Tsili, and A. G. Kladas, "Transformer design and optimization: A literature survey," *IEEE Trans. Power Del.*, vol. 24, no. 4, pp. 1999–2024, Oct 2009.

[6] R. Petkov, "Optimum design of a high-power, high-frequency transformer," *IEEE Trans. Power Electron.*, vol. 11, no. 1, pp. 33–42, Jan 1996.

[7] W. G. Hurley, W. H. Wolfle, and J. G. Breslin, "Optimized transformer design: inclusive of high-frequency effects," *IEEE Trans. Power Electron.*, vol. 13, no. 4, pp. 651–659, Jul 1998.

[8] G. Ortiz, J. Biela, and J. W. Kolar, "Optimized design of medium frequency transformers with high isolation requirements," in *IECON 2010 - 36th Annu. Conf. on IEEE Ind. Electron. Soc.*, Nov 2010, pp. 631–638.

[9] P. Shuai and J. Biela, "Design and optimization of medium frequency, medium voltage transformers," in *2013 15th European Conf. on Power Electron. and Applicat. (EPE)*, Sept 2013, pp. 1–10.

[10] M. A. Bahmani, T. Thiringer, and M. Kharezy, "Optimization and experimental validation of medium-frequency high power transformers in solid-state transformer applications," in *2016 IEEE Appl. Power Electron. Conf. and Expo. (APEC)*, March 2016, pp. 3043–3050.

[11] ——, "Design methodology and optimization of a medium-frequency transformer for high-power dc-dc applications," *IEEE Trans. Ind. Appl.*, vol. 52, no. 5, pp. 4225–4233, Sept 2016.

[12] I. Villar, "Multiphysical characterization of medium-frequency power electronic transformers," Ph.D. dissertation, EPFL, Switzerland, 2010.

[13] I. Villar, L. Mir, I. Etxeberria-Otadui, J. Colmenero, X. Agirre, and T. Nieva, "Optimal design and experimental validation of a medium-frequency 400kva power transformer for railway traction applications," in *2012 IEEE Energy Conversion Congr. and Expo. (ECCE)*, Sept 2012, pp. 684–690.

[14] [Online]. Available: http://www.metglas.co.in/

[15] [Online]. Available: http://www.dupont.co.in/

[16] C. P. Steinmetz, "On the law of hysteresis," *Trans. of the Amer. Inst. of Elect. Engineers*, vol. IX, no. 1, pp. 1–64, Jan 1892.

[17] P. L. Dowell, "Effects of eddy currents in transformer windings," *Elect. Engineers, Proc. of the Institution of*, vol. 113, no. 8, pp. 1387–1394, August 1966.

[18] G. S. Dimitrakakis and E. C. Tatakis, "High-frequency copper losses in magnetic components with layered windings," *IEEE Trans. on Magnetics*, vol. 45, no. 8, pp. 3187–3199, Aug 2009.

[19] M. A. Bahmani, T. Thiringer, and H. Ortega, "An accurate pseudoempirical model of winding loss calculation in hf foil and round conductors in switchmode magnetics," *IEEE Trans. Power Electron.*, vol. 29, no. 8, pp. 4231–4246, Aug 2014.

[20] A. K. Das, H. Tian, Z. Wei, V. B. Sriram, S. Cao, A. Tripathi, and P. C. Kjær, "Accurate calculation of winding resistance and influence of interleaving to mitigate ac effect in a medium-frequency high-power transformer," in *2017 Asian Conf. on Energy, Power and Transportation Electrification (ACEPT)*, 2017, in press.

[21] I. Villar, U. Viscarret, I. Etxeberria-Otadui, and A. Rufer, "Transient thermal model of a medium frequency power transformer," in *2008 34th Annu. Conf. of IEEE Ind. Electron.*, Nov 2008, pp. 1033–1038.

[22] A. K. Das, Z. Wei, V. B. Sriram, S. Cao, H. Tian, A. Tripathi, and P. C. Kjær, "Thermal modeling and transient behavior analysis of a medium-frequency high-power transformer," in *IECON 2017 - 43rd Annu. Conf. of the IEEE Ind. Electron. Soc.*, 2017, in press.

[23] R. K. Arora, *Optimization Algorithms and Applications*. Boca Raton, FL: CRC Press, 2015.

[24] [Online]. Available: http://www.ansys.com/